Photogenerated Charge Carriers Dynamics on La and/or Cr Doped $SrTiO_3$ Nanoparticles Studied by Transient Absorption Spectroscopy

Fumihiko Ichihara[†, ‡], Fabian Sieland[§, ∥], Hong Pang[†, ‡], Davin Philo[†, ‡], Anh-Thu Duong[§, ○], Kun Chang[†, ⊥], Tetsuya Kako[†], Detlef W. Bahnemann[§], Jinhua Ye[†, ‡, Δ]*

† International Center for Materials Nanoarchitectonics (WPI-MANA), National Institute for Materials Science (NIMS), 1-1 Namiki, Tsukuba, Ibaraki 305-0044, Japan.

‡ Graduate School of Chemical Sciences and Engineering, Hokkaido University, Sapporo 060-0814, Japan.

§ Institute for Technical Chemistry, Leibniz University Hannover, Hannover 30167, Germany.

⊥ College of Materials Science and Technology, Jiangsu Key Laboratory of Materials and Technology for Energy Conversion, Nanjing University of Aeronautics and Astronautics, Nanjing 211100, P. R. China.

Δ TJU-NIMS International Collaboration Laboratory, School of Materials Science and Engineering, Tianjin 300072, P. R. China.

ABSTRACT

Elemental doping into semiconductor-based photocatalysts to narrow the bandgap and extend the light absorption to visible light region is a conventional strategy widely adopted. However, one critical problem but rarely addressed is the drastically decreased photocatalytic activity under UV light despite of the increased activity in visible light region, resulting in a decreased total performance under full solar spectrum. In order to elucidate the origin of the commonly observed phenomena, herein we choose La, Cr-codoped $SrTiO_3$ as a proof-of-concept model to probe the effect of dopants on the behavior of photogenerated charge carriers by transient absorption spectroscopy. By observing the excitons, it is found that under UV irradiation, the excitation occurring from the Cr impurity bands limits the excitation of $SrTiO_3$ from valence band, causing the drastic decrease of the photocatalytic activity over doped material. The widely proposed recombination at dopant sites, however, is not dominant for declining the UV light-irradiated performance, especially in the presence of reactant gas (methanol vapor).

1 INTRODUCTION

Photocatalytic production of solar fuels from water splitting[1-5], CO_2 reduction[6-10], and nitrogen fixation[11-12] has become a major research topic in solar energy conversion. New photocatalysts are continually being designed to demonstrate their capabilities for effective light absorption and conversion. In most reports, taking into consideration that the ultraviolet light only accounts for 4 % of the solar spectrum[1, 13], the extended light absorption into visible light over the developed photocatalysts was emphasized. Among the strategies including photosensitization[14-15], doping[2, 16], localized surface plasmon resonance[6, 17], etc., extrinsic elemental doping into the semiconductor-based photocatalysts to narrow the bandgap is a conventional and useful method widely engaged by the researchers. Taking TiO_2 and $SrTiO_3$ as examples, doping of transition metals[18-21], nitrogen[22-23] and sulfur[24] have been extensively carried out. It is reported that by doping, impurity bands are created which enable the absorption of visible light to excite electrons.[2-3, 18-24] However, one of the critical problems but rarely addressed is the change of the light absorption and photocatalytic activity under UV light region. In fact, the photocatalytic activity under UV light is drastically decreased after doping even though their performance under visible light could be enhanced, resulting in a lower total photocatalytic activity under the full spectrum of solar light irradiation.[25-27] The only exception is that doping of lanthanides and alkali earth metals into $SrTiO_3$ and TiO_2 seems to enhance the photocatalytic activities under UV light irradiation, leading to the improved total photocatalytic activity under full solar spectrum.[16, 28]

It is widely believed that the unoccupied d-orbital of transition metals may form some mid-gap states which can capture electrons and holes together, acting as a recombination center.[29-30] But the actual role of dopants and how they affect the charge carriers dynamics has not yet been fully

elucidated. To restrain the negative drawbacks of the lattice mismatching or valence state unbalance by monodoping, codoping is often used beyond monodoping, which makes the charge carriers dynamics more complicated. In this regard, to investigate the function of dopants for regulating the photocatalytic activity is imperative to design and fabricate a UV and visible light active photocatalyst.

Transient absorption spectroscopy (TAS) is a well-known powerful technique to monitor the photo-excited charge carrier trapping and lifetime in the semiconductors.[31-32] In TAS measurements, the transient changes in absorption are tracked after irradiation of pulse light for excitation. By monitoring this absorption, the decay kinetics of photo-generated charge carrier trapping as well as recombination process can be studied. The time resolved absorption has been applied to elucidate the charge carriers dynamics in TiO_2[30, 33], $NaTaO_3$[34], $SrTiO_3$[35-36], $LaTiO_2N$[37] and $Ba_5Ta_4O_{15}$.[31] However to our knowledge, there are only few reports on the doped materials.[25, 38]

As one of the reports, Yamakata et al. assumed that the recombination occurring on Ni might be the reason which caused the decreased photocatalytic activity over Ni, Ta-codoped $SrTiO_3$.[25] But later they found that Ni is not the main recombination center via TAS observation of the charge carrier dynamics. Onishi et al. also applied TAS measurements over Rh, Sb-codoped $SrTiO_3$. Even though monodoped Rh^{4+} was demonstrated to be the recombination center, after charge compensation by Sb^{5+} codoping, the recombination on Rh^{3+} was suppressed. And the suppressed recombination could not trigger the photocatalytic H_2 evolution reaction (HER) performance. Instead the photocatalytic HER activity decreased to less than one third.[38] Why the photocatalytic activity of the codoped $SrTiO_3$ reduced under UV light still remains a pending question.

In our previous effort to extending light absorption of $SrTiO_3$ to visible light region[18], we found that Cr doping is an effective way to red-shift the light absorption because of the Cr^{3+} energy state located at 2.2 eV lower than the bottom of conduction band of $SrTiO_3$.[39] However, Cr^{6+} state often occurs in the Cr mono-doped $SrTiO_3$, which diminishes the photocatalytic activity due to the unoccupied Cr^{6+} state with a potential lower than that for HER performance. To restrain the formation of Cr^{6+}, codoping with Sb, Ta, Nb and W was proposed to suppress the formation of defects and to maintain the charge neutralization.[2, 4, 40-41] Later, we demonstrated that codoping with lanthanum (La) is more promising compared with other elements to stabilize the Cr^{3+} for HER under visible light irradiation[42], from a systematic study combining experiments and theoretical calculation.

Herein, we choose the La and/or Cr doped $SrTiO_3$ as a proof-of-concept model to examine the effects of doping on the carrier dynamics within nano-micro seconds regime. By using the TAS measurements, the trapped charge carriers were probed in the visible light range in the presence of the electrons and holes scavengers. The effects of dopants on velocity of the carriers in the photocatalytic reaction and the recombination were investigated. This work provides a deep understanding charge carrier dynamics over La, Cr doped $SrTiO_3$ which suggested the origin of enhancing photocatalytic activity by La doping and decreasing the photocatalytic activity by Cr doping under UV light irradiation.

2 EXPERIMENTAL METHODS

2.1 **Materials and synthesis**

$SrTiO_3$ nanoparticles were synthesized by a polymerizable complex (PC) method.[13] In brief, $Ti(OC_4H_9)_4$ (Sigma-Aldrich, 99.9%) was dissolved into ethylene glycol and continuously stirred

for 30 minutes under nitrogen atmosphere. Afterwards, $Sr(NO_3)_3$ (Sigma-Aldrich, 99.9%) and citric monohydrate (Carl Roth, 99.5%) were added; the stirring was continued until the solution became entirely transparent (denoted as solution A). For doping of lanthanum and chromium, $La(NO_3)_3 \cdot 6H_2O$ (Sigma-Aldrich, 99.9%) and $Cr(NO_3)_3 \cdot 9H_2O$ (Sigma-Aldrich, 98%) were separately dissolved into 2-methoxymethnol (Sigma-Aldrich, 98%). The required stoichiometric amount of these solutions with the concentration of 0.05 mol/L was added into solution A. The reaction mixture was subsequently stirred for 15 minutes to achieve the dissolution of reagents, and then heated at around 120 ˚C for 5 h to promote polymerization. During the heating process, the solvent was evaporated and the suspension turned into a transparent brownish resin. The resin was further heated at 350 ˚C for 3 h with slow heating rate (1 ˚C/min). Subsequently, the resulted cinders were ground to obtain fine nanoparticles, and further calcined at 750 ˚C for 6 hours.

It should be stated here that in La, Cr-codoped $SrTiO_3$, the doping amounts were ca. 3%. For investigation of monodoped effect of either La or Cr on $SrTiO_3$, a higher doping amount (12%) was applied to magnify the effects of dopants.

2.2 **Characterization**

The transient absorption system set-up used in this work is described in the literature.[31] In brief, Q-switched Nd: YAG laser (Quantel; Brilliant B, third harmonics, 355 nm, 10 Hz) was used as an excitation light with the duration time of 20 ns. The employed excitation laser spot size was 0.75 cm^2, the calculated fluence would be 1.33 mJ/cm^2. After the sample was irradiated by the excitation light, 150 W Xe lamp (Osram XBO; 150 W) was applied as the probe light source for analyzing the absorption of transient species. Probe light was focused onto solid

samples surface by using two plane folding mirrors and lens. The diffusely reflected probe light was collected by a different set of lens and plane folding mirror leading to a monochromator. Then, the dispersed light from the monochromator fell into photomultiplier detector (Hamamatsu R928 photomultiplier), which would convert the optical signals to electric signals; these signals were subjected into the distal oscilloscope via tunable signal terminator. The oscilloscope recorded the data points as voltage changes, which can be recalculated to transient absorption, ΔJ, according to following equation: (eq 1)

$$\Delta J = (J_0 / I_0 - J_x / I_0) / (J_0 / I_0) = (J_0 - J_x) / J_0 \qquad (1)$$

, where I_0 is the light intensity of probe light, J_0 is the signal intensity of diffusely reflected probe light without the excitation, and J_x is the signal of diffusely reflected probe light with irradiation of the excitation laser pulse.

The recorded decay signal ΔJ was fitted to a fractal fit function[33] (eq 2)

$$\Delta J = A\,(1-h) / [(1-h) + A k_{2,f}\, t^{1-h}] \qquad (2)$$

, where A represents the intensity of transient signals, and the exponent h represents the fractal dimension of the surface; the decay constant $k_{2,f}$ is related to charge carriers trapping and recombination.

For the transient absorption experiments, the powder photocatalysts were packed in the quartz cuvette which allowed the introduction of reactant gases. Here O_2 gas and MeOH vapor were applied as electrons and holes scavengers, respectively.

The optical properties of powders were recorded by the diffuse reflectance spectroscopy in the range of 270-850 nm over V-570 UV/Vis Spectrophotometer (JASCO Corp, Japan) equipped with an integrating sphere and a $BaSO_4$ reference. The measured reflectance data were converted to absorbance via the Kubelka-Munk function. The X-ray powder diffraction (XRD) measurements were performed on an X-ray diffractometer (X'pert powder, PANalytical B.V., Netherlands) with a Bragg Brentano geometry using Cu Kα radiation. High-resolution transmission electron microscopy (HR-TEM) measurements were performed using JEM-2010 with an acceleration voltage of 200 kV. The core-level photoelectron spectra were recorded by X-ray photoelectron spectroscopy (XPS; VG-ESCA Mark II), in which Mg Kα radiation (1253.6 eV) and a pass energy were employed at 200 W and 100 eV, respectively. The charge-up of the binding energy values was referenced to the C-C bond of adventitious carbon contamination in the C 1s peak at 284.8 eV as the internal standard. Quantitative analyses were performed by comparing relative areas taking into consideration of the atomic sensitivity factor for the corresponding elements.

The photocatalytic H_2 reductions were carried out in a Pyrex glass reaction cell linked to a gas-closed circulation system connected to a gas chromatography (GC) (GC-8A, Shimadzu Co., Japan, Carrier gas: Ar) with a thermal conductivity detector (TCD) for online analysis of the H_2 production. 100 mg of photocatalyst were put into 300 mL of 10 vol% methanol aqueous solution and subjected to some ultrasonic treatment prior to the photocatalytic measurement.

3. RESULTS AND DISCUSSION

3.1 **Steady state characterization of the La and/or Cr doped $SrTiO_3$**

Figure 1a shows the powder XRD patterns of synthesized catalysts. The XRD patterns exhibited that all samples reflect cubic perovskite symmetry. In perovskite (ABO_3) structure, cations with larger ionic radius generally occupy A site and the smaller one occupy B site. Thus, it is considered that Sr and La cations have 12 coordination to oxygen atoms, while Ti and Cr cations have octahedral coordination with 6 oxygen atoms. Figure 1b shows the magnified 110 diffraction peak of the doped and the undoped $SrTiO_3$. In this case, the ionic radius of La (1.40 Å) is smaller than that of Sr (1.44 Å), while the ionic radius of Cr (0.615 Å) is bigger than that of Ti (0.605 Å), the corresponding peak position of La, Cr-codoped $SrTiO_3$ is found to be close to that of the undoped $SrTiO_3$. Goldschmidt[43] has introduced a tolerance factor (t), defined by the equation: $t = (r_A+r_O) / [(r_B+r_O)\sqrt{2}]$ (r_A, r_B, and r_O are the empirical ionic radii of A, B, O atoms in ABO_3 at room temperature), to evaluate the deviation of $SrTiO_3$ from the ideal structure. The t values of $SrTiO_3$, La-doped $SrTiO_3$, Cr-doped $SrTiO_3$ and La, Cr-codoped $SrTiO_3$ were calculated to be 0.9986, 0.9958, 0.9981 and 0.9983, respectively, all of which are within the allowed t values (0.75 to 1.0)[44]. So, it is further confirmed that there is no significant distortion in the $SrTiO_3$ crystal structure by doping.

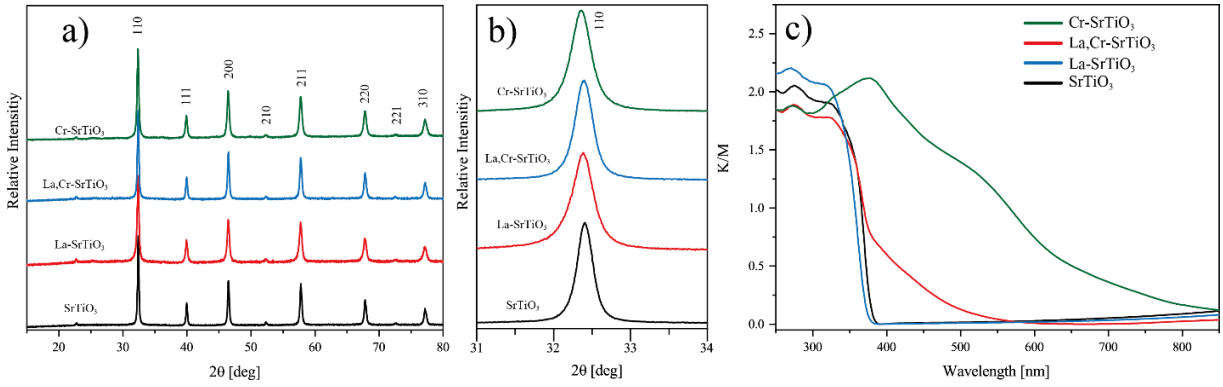

Figure 1. (a) XRD patterns and (b) (110) facet (c) UV-Vis spectra of doped and pure $SrTiO_3$.

Figure 1c shows the absorption spectra of the La and/or Cr doped $SrTiO_3$ powders. The undoped and La-doped $SrTiO_3$ can only absorb UV light with wavelength less than 400 nm. However, La, Cr-codoped $SrTiO_3$ and Cr-doped $SrTiO_3$ exhibited strong absorption in the visible light region (400-580 nm for La, Cr-codoped $SrTiO_3$ and 400-850 nm for Cr-doped $SrTiO_3$). A broad absorption band at 400-600 nm can be assigned to the charge transfer absorption from Cr^{3+} to Ti^{4+}, while the absorption at 580-750 nm can be assigned to the upward d-d transition of $^4A_2 \rightarrow {}^4T_2$ in Cr^{3+} cations in octahedral units, indicating that a part of Cr cations would form tri-valence state in $SrTiO_3$.[45-46] In contrast, Cr-doped $SrTiO_3$ exhibited an additional absorption band over 700 nm, due to the presence of incorporated vacancy by Cr^{6+}.[3, 19] It is reported that Cr^{3+} state is beneficial for photocatalytic HER.[2, 18] The doped Cr cations will induce an absorption band over 400 nm, which is caused by electrons excitation from d-orbital of Cr cations to the conduction band of $SrTiO_3$. This optical transition is necessary for the photocatalytic activity under visible light irradiation.

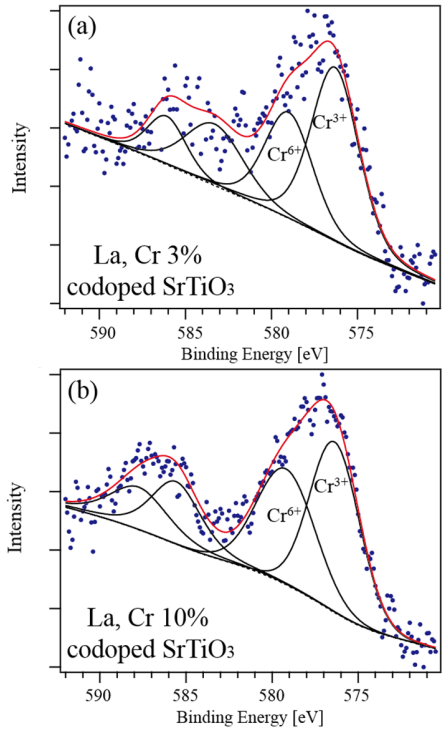

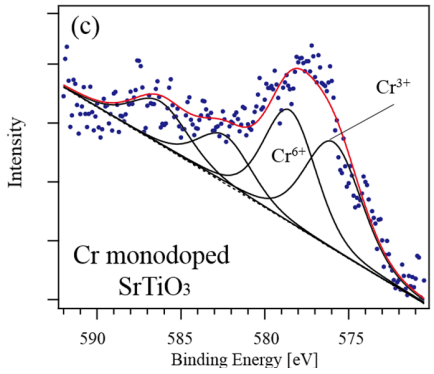

	Cr^{3+}	Cr^{6+}
La, Cr 3% codoped $SrTiO_3$	62.1%	37.9%
La, Cr 10% codoped $SrTiO_3$	60.4%	39.6%
Cr-doped $SrTiO_3$	50.2%	49.8%

Figure 2. XPS spectra of Cr 2p in the Cr-doped $SrTiO_3$ and La,Cr-codoped $SrTiO_3$.

Cr 2p XPS for 3%, 10% La, Cr-$SrTiO_3$, and Cr-doped $SrTiO_3$ are shown in Figure 2. The Cr 2p spectra allow us to tentatively assign the oxidation states of the Cr dopants. The binding energies and the multiplet splitting of the $2p_{3/2}$ peak at ~575−577 eV in the 3%, 10% La, Cr-$SrTiO_3$ suggest that the majority of Cr dopants are in the Cr^{3+} state. However, Cr-doped $SrTiO_3$ shows nearly equivalent intensity in the binding energy range characteristic of higher oxidation states Cr^{6+} (578−580 eV) with the Cr^{3+} state.

3.2 **Photocatalytic activity of the samples**

The photocatalytic HER activity was evaluated by suspending the synthesized catalysts (loaded by 1.0 wt% Pt cocatalyst) in 10 vol% methanol aqueous solution. Figure 3 shows the hydrogen evolution over the synthesized catalysts under visible light (420 nm cut off filter) and

full-arc (UV+Vis) light irradiation, respectively. Under visible light irradiation, only negligible amount of H_2 evolved over the undoped $SrTiO_3$ (< 1 μmol/h) as expected from its wide band gap. However, the rate of HER of La, Cr-codoped $SrTiO_3$ increased to 7.97 μmol/h, in a good accordance with those previously reported for doped $SrTiO_3$.[25, 38] In contrast, under the UV + Vis light irradiation, La, Cr-codoped (15.9 μmol/h) and Cr-doped (2.69 μmol/h) $SrTiO_3$ showed much lower activity compared to La-doped $SrTiO_3$ (550.4 μmol/h) and the undoped $SrTiO_3$ (379.2 μmol/h).

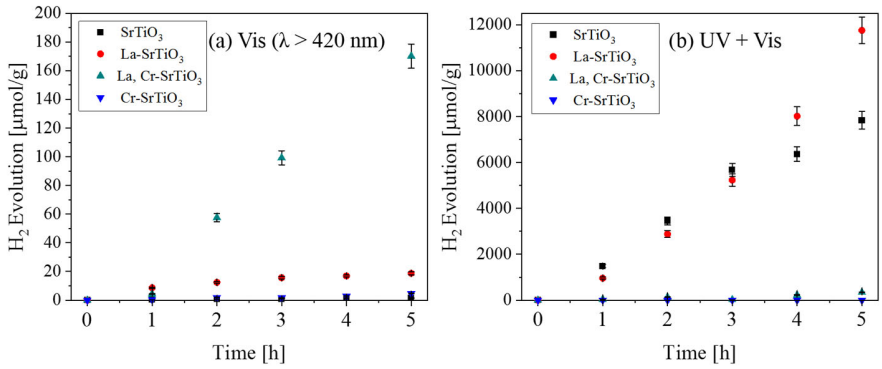

Figure 2. (a) Photocatalytic HER under visible light irradiation (b) UV+Vis light irradiation.

3.3 **Behavior of photogenerated charge carriers in undoped $SrTiO_3$**

In order to determine the effects of doping on the photocatalytic activity, transient absorption spectra of the undoped $SrTiO_3$ were firstly measured upon UV pulsed laser (355 nm) irradiation in N_2 atmosphere. The measurement was performed in the wavelength range of 400-850 nm whereby the transient absorption signal of trapped electrons and holes are usually generated. In this kind of measurement, the intensity of the signal which corresponds to trapped electrons will decrease drastically when electron scavenger is applied. Meanwhile, in the situation where hole scavenger is utilized, slow kinetics of trapped electrons will be observed (preservation of the

signal), since the electrons cannot recombine with the photogenerated holes. In contrast, the signal for trapped holes will last long after the addition of electron scavenger, indicating prolonged lifetime of holes due to the deceleration of recombination process. Besides, the transient absorption decay curve will display a fast decay characteristic of the holes signal in the presence of hole scavenger.

As shown in Figure 4a, at least two broad absorption bands can be observed at 825 nm and 765 nm, which can be assigned to the charge carries that were gravitated towards the trapping states in the band gap. The detailed decay processes ΔJ of the transient absorption bands recorded at 825 and 765 nm were further investigated in the presence of O_2 gas and methanol (MeOH) vapor, which work as the electron and hole scavengers, respectively.[47-48] As shown in Figure 5a, the transient absorption intensity decay curves at 765 nm were fitted in 0−400 μs scale by eq 2. In the presence of hole scavenger MeOH, the signal intensity A drastically decreased to 0.68 from 7.70 in N_2 atomosphere. Meanwhile, the decay constant $k_{2,f}$ increased to 0.06, about 5 times higher than those in the N_2 and O_2 environment (0.012 and 0.013, respectively) due to hole-consuming reaction by MeOH. In contrast, in the presence of electron scavenger O_2, the signal intensity increased to 8.08, and the $k_{2,f}$ became slightly lower by electron-consuming reaction of O_2. Thus, the transient absorption signal at 765 nm can be assigned to the population of photogenerated holes. As the absorption band at 825 nm also shows similar trend in the presence of MeOH vapor and O_2 gas, the transient absorption at 825 nm was also assigned to the signal of holes (See supporting information Figure S1). These highly reactive photogenareted holes in the undoped $SrTiO_3$ contribute to the photocatalytic activity under UV light irradiation.

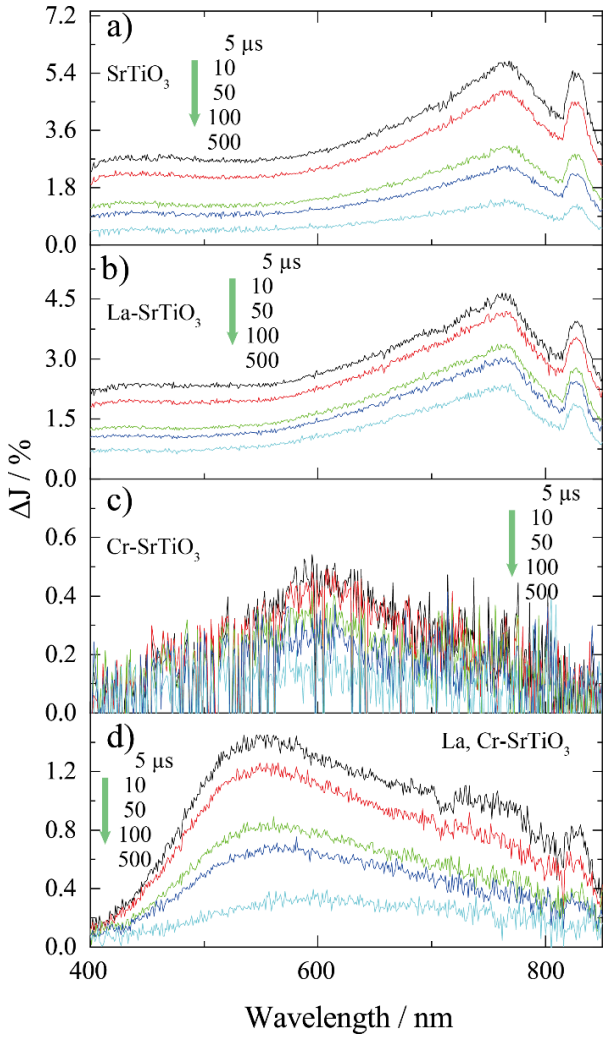

Figure 4. (a) Transient absorption spectra of $SrTiO_3$ (a), La-$SrTiO_3$ (b), Cr-$SrTiO_3$ (c), 3% La, Cr-$SrTiO_3$ (d) particles irradiated by UV (355 nm) pulsed laser under N_2 gas. The pump energy was 1.0 mJ/pulse, and the repetition rate was 10 Hz.

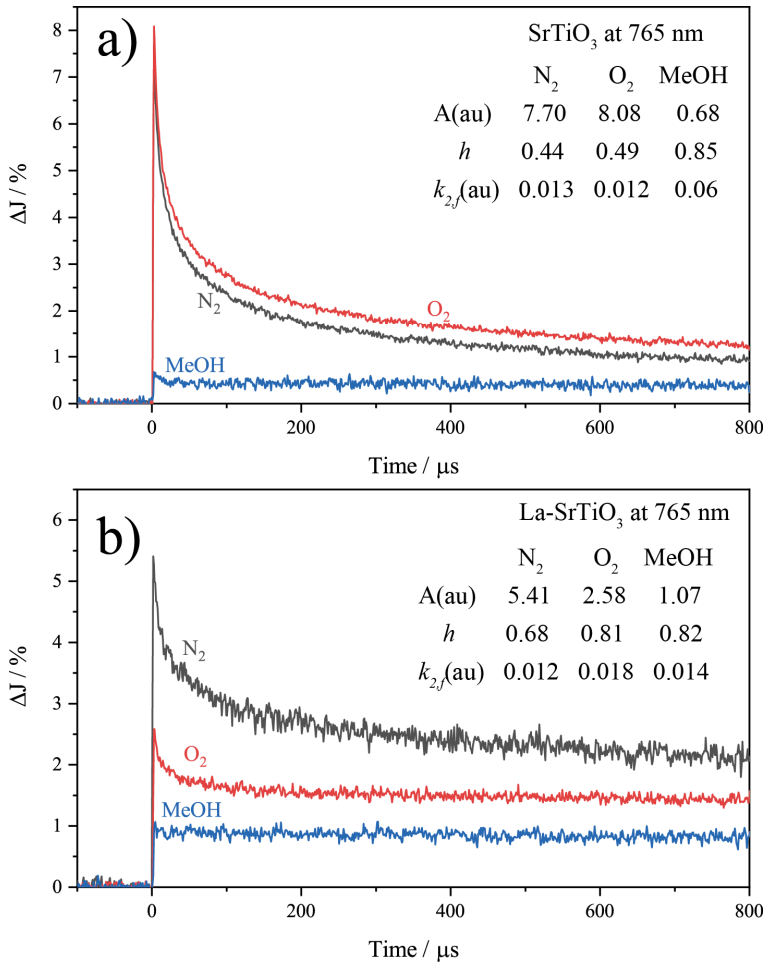

Figure 5. Decay curves of transient absorption of the $SrTiO_3$ at 765 nm (a), La-$SrTiO_3$ at 765 nm (b).

3.4 **Effect of La doping**

The transient absorption spectral shape of La-doped $SrTiO_3$ (Figure 4b) was in resemblance to that of $SrTiO_3$. However, La-doped $SrTiO_3$ exhibited different decay processes of the transient absorption bands at 825 and 765 nm compared to those of the undoped $SrTiO_3$ where the signal reflects the population of photogenerated holes. As shown in Figure 5b, in the presence of hole

scavenger MeOH, vapor the signal intensity of transient absorption exhibited the fastest decrease, similar to those observed in the undoped $SrTiO_3$. Interestingly, the signal observed in the presence of O_2 gas also showed faster decrease compared with that in N_2 gas. The above results suggest that transient absorption of La-doped $SrTiO_3$ in the visible light region reflects the quantity of both photogenerated electrons and holes. Why the transient species at 765 nm and 825 nm have been changed to both trapped electrons and holes, different with only holes in the undoped $SrTiO_3$? It is suggested that the trapped electrons could absorb the probe light (765 nm and 825 nm), and hence be excited to La 5d bands which are associated with Ti 3d orbital when La is doped at the Sr site of $SrTiO_3$.[49]

To prove the effect of La doping on recombination kinetics, the normalized decay processes of the undoped $SrTiO_3$ and La-doped $SrTiO_3$ at 765 nm in the presence of N_2 gas were compared as shown in Figure 6. Since there is no molecules that photogenerated charge carriers can react with, the decay processes should reflect the intrinsic recombination kinetics within the undoped $SrTiO_3$ and La-doped $SrTiO_3$.[50] According to the fitting results of the decay curves, La doping can improve the decay constant $k_{2,f}$ value which is implicated in prolonging the carriers lifetime in each arbitrary time scale (0 to 50 μs, 50 to 100 μs and 100 to 400 μs), owing to its ability to secure the photogenerated charge carriers.[49, 51-52] As the longer lifetime carriers have higher probability of taking part in the photocatalytic reaction than the shorter lifetime carriers, it is understandable that the photocatalytic activity of the La-doped $SrTiO_3$ increased under UV+Vis light irradiation (Figure 3b).

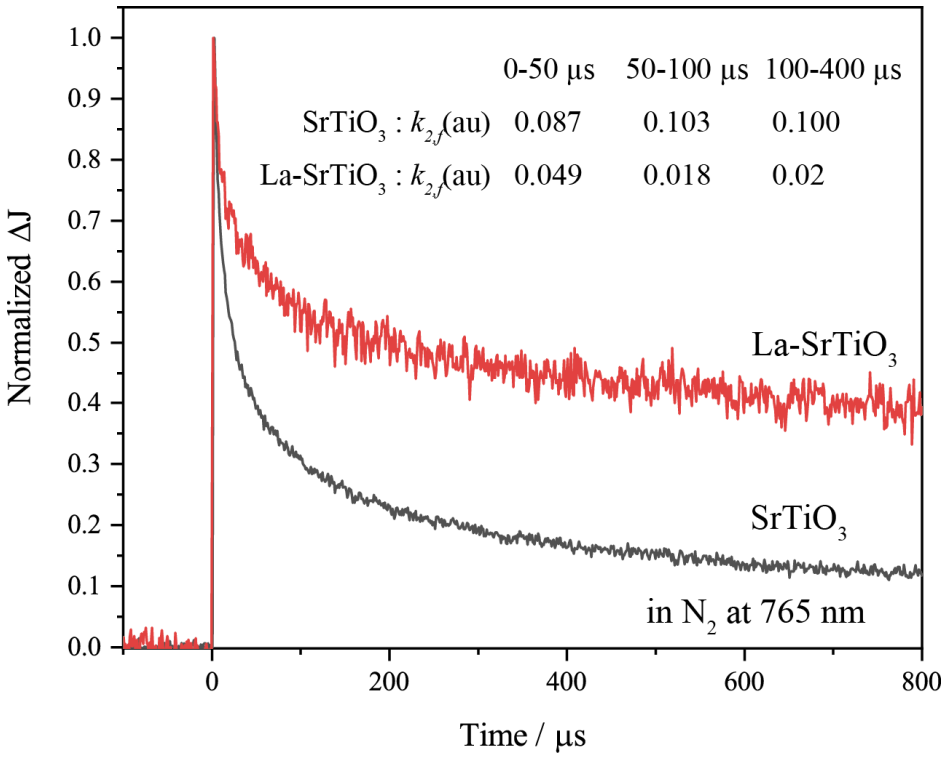

Figure 6. Comparison of the normalized decay curves of the undoped $SrTiO_3$ and La-$SrTiO_3$ in N_2 ambient at 765 nm.

The above results imply that those dopants which can form and hybridize the impurity level with the conduction band of the semiconductor, will be beneficial for securing the carriers and prolonging the lifetime of the photogenerated carriers, rather than acting as recombination center.[53]

3.5 **Effect of Cr doping**

Since Cr doping can significantly affect the band structure of $SrTiO_3$, the corresponding transient absorption spectra have a drastic change compared to the original one as seen from Figure 3c. It is found that the absorption bands at 825 nm and 765 nm are dumped since the Cr impurity levels are located in the band gap of the $SrTiO_3$ and may overlap with the trapping

states of holes. Instead, a new broad absorption band with the peak at around 600 nm can be observed. XPS spectra (Figure 2) indicate that Cr with two different valence states (Cr^{3+} and Cr^{6+}) coexisted in Cr-doped $SrTiO_3$ in a nearly equivalent amount. This newly emerged absorption band can be therefore attributed to the inserted Cr^{3+} and Cr^{6+} impurity level between valence band top and conduction band bottom.

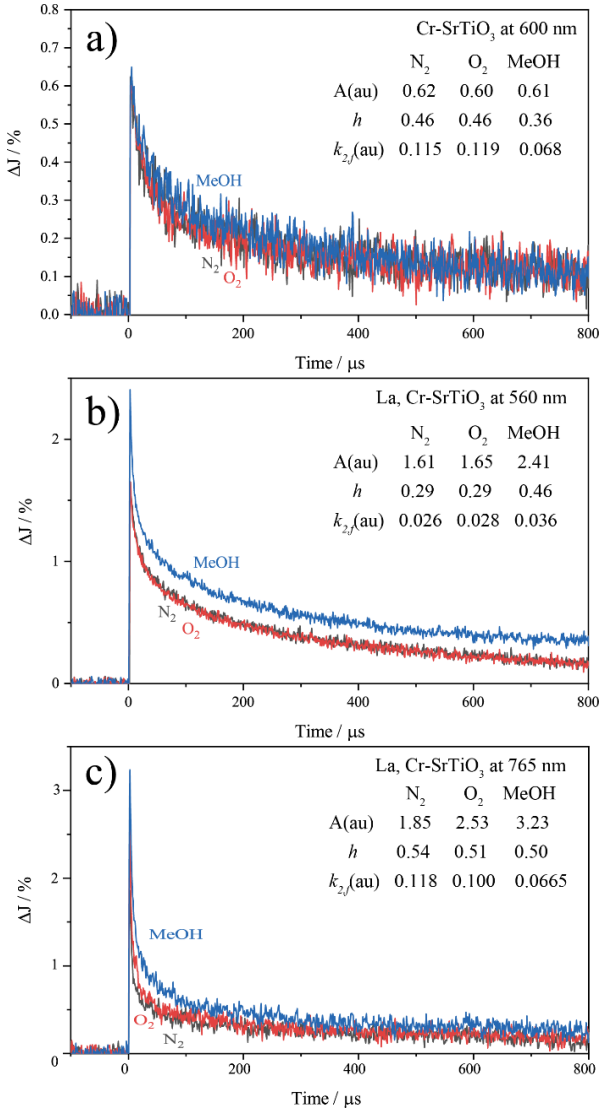

Figure 7. Decay curves of transient absorption of the Cr-$SrTiO_3$ at 600 nm (a), 3% La, Cr-$SrTiO_3$ at 560 nm (b) and 765 nm (c).

As shown in Figure 7a, in the presence of hole scavenger MeOH, the decay constant $k_{2,f}$ decreased to half of the value in N_2 and O_2, indicating that the decay process of the absorption maxima at 600 nm was decelerated. According to what we mentioned above in section 3.3, this transient absorption signal mainly reflected the population of photogenerated electrons. But when exposed to electron scavenger O_2 gas, the decay process seldom changed, suggesting that the photogenerated electrons have no reactivity compared with charge carriers in $SrTiO_3$ and those in La-doped $SrTiO_3$. This lost reactivity is possibly the main reason for the drastic decrease in photocatalytic HER activity over Cr-doped $SrTiO_3$.

3.6 **Effect of La and Cr co-doping**

The 3% La, Cr-codoped $SrTiO_3$ was then measured by TAS. As shown in Figure 4d, the transient absorption spectra exhibited feature of transient absorption signals derived from $SrTiO_3$ around 825 nm and 765 nm, while the new broad absorption with the peak top at 560 nm has been emerged. The transient absorption spectrum shape at 3 μs reflected both features which observed in transient absorption spectra over the undoped $SrTiO_3$ (Figure 4a) and Cr-doped $SrTiO_3$ (Figure 4c). Interestingly, the peak of transient absorption signal appeared at 560 nm initially (3 μs), but shifted to 600 nm (500 μs) gradually along with the time proceeded, approaching to the shape of Cr-doped $SrTiO_3$ finally. This kind of decay kinetic of La, Cr-codoped $SrTiO_3$ indicated charge carriers consuming reaction occurred in the measurement time domain (within 500 μs). Considering the fact that Cr^{6+} co-existed with Cr^{3+} equivalently in the Cr doped $SrTiO_3$, but was much suppressed by La doping in either 3% La, Cr-codoped $SrTiO_3$ (Figure 4d) and 10% La, Cr-codoped $SrTiO_3$ (Figure S2), the peak shift in transient absorption signal from 560 to 600 nm might be attributed to the valence change of Cr^{3+} to Cr^{6+} by trapping three holes.[13] To confirm if the transient absorption peak position at 560 nm is assigned to the

Cr^{3+} impurity level, we further conducted TAS measurement by using a sample with higher doping amount (10% La, Cr-codoped $SrTiO_3$). The shape of the transient absorption spectra (See Figure S2) resembled with Cr-doped $SrTiO_3$ (Figure 4c), however, the apex blue-shifted from 600 nm to 560 nm, indicating that the trapping state of Cr^{3+} impurity levels are located deeper than Cr^{6+} level. The peak shift of transient absorption along with time was not obvious in this case, probably because a part of Cr^{3+} cations in 10% La, Cr-codoped $SrTiO_3$ still remains tri-valence state due to much increased Cr doping amount.

To understand the role of Cr in La, Cr-codoped $SrTiO_3$, the decay curves of transient absorption at 560 nm and 600 nm were investigated in N_2 gas and MeOH vapor, respectively. As shown in Figure 8a, in the inert N_2 gas, the signal at 560 nm derived from Cr^{3+} decays faster than the signal of Cr^{6+} (at 600 nm). This suggests that Cr^{3+} doped into $SrTiO_3$ would trap 3 holes and hence change to Cr^{6+}. However, the reverse phenomenon where Cr^{6+} trapped three photoexcited electrons and reverted to Cr^{3+} again couldn't be observed within the range up to 800 μs. On the other hand, while MeOH vapor existed in the measurement environment (as hole scavengers), the decay curves were almost the same for both 560 nm and 600 nm wavelength (Figure 8b). Since the photogenerated holes by laser irradiation were instantaneously captured by MeOH vapor, consequently the Cr^{3+} cations were not able to trap the photogenerated holes. Thus in this situation, the decay curve at 560 nm derived from Cr^{3+} mainly follows the thermal equilibrium, similar to the one at 600 nm derived from Cr^{6+}. This suggests that in the photocatalytic HER evaluation with methanol as sacrificial agent, the Cr^{3+} would not act as the recombination center and therefore couldn't be considered as the main reason for the decrease in photocatalytic activity under UV light irradiation.

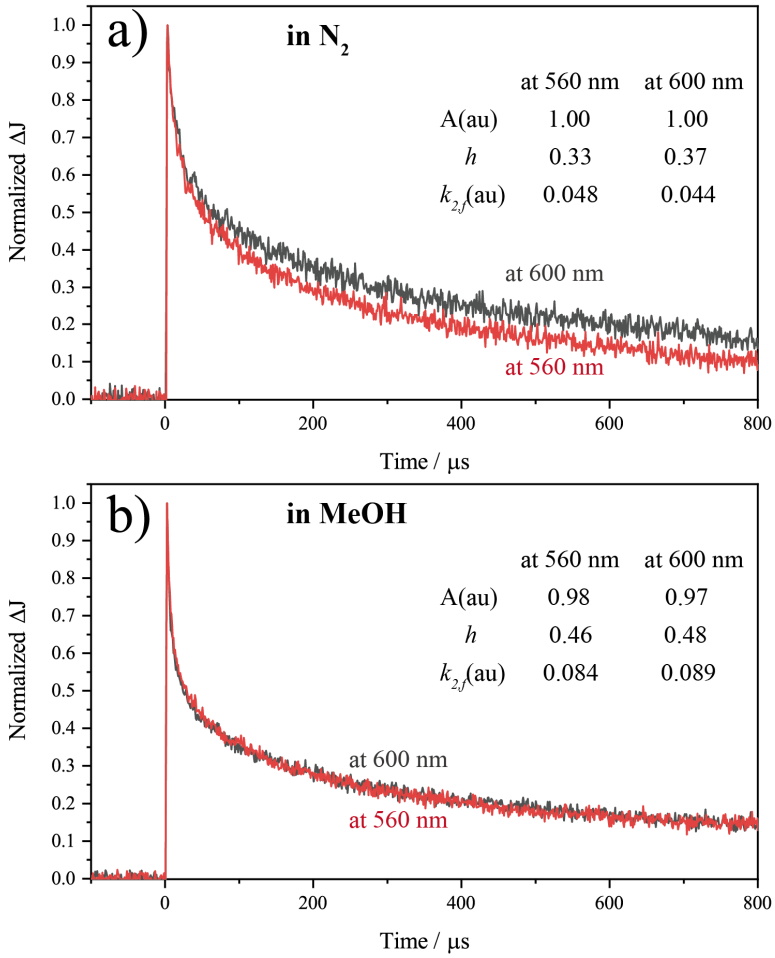

Figure 8. The comparison of 3% La, Cr-$SrTiO_3$ at 600 and 560 nm in N_2 ambient (a) and MeOH vapor (b).

To evaluate the effects of La and Cr codoping on the carriers property of $SrTiO_3$, the decay curves at 765 nm (where $SrTiO_3$ exhibits the absorption maxima on transient absorption spectra) are essential for analyzing the recombination kinetics. As shown in Figure 6b, the transient absorption spectra around 765 nm preserve part of the feature of the undoped $SrTiO_3$, hence similar reactivity might be expected from La, Cr-codoped $SrTiO_3$. However, the decay processes shown in Figure 7c reveal that the reactivity of the corresponding charge carriers was quite different from that of the undoped $SrTiO_3$ (Figure 5a) and La-doped $SrTiO_3$ (Figure 5b). In

MeOH, the signal intensity relatively increases compared with that in N_2 and displays trapped electrons tendency, while the undoped $SrTiO_3$ displays holes tendency. This implies that $SrTiO_3$ was not sufficiently excited by UV laser irradiation and the majority of excitation originated from the Cr impurity band in La, Cr-codoped $SrTO_3$. This is probably because Cr cations occupy oxygen octahedral coordination center, and the electronic structure of the predominantly O 2p-derived valence band has been affected by Cr doping. Correspondingly, UV-Vis spectra (Figure 1c) also show that the absorption intensity in the UV light region decreases after Cr doping and La, Cr codoping.

Furthermore, in oxygen environment, the decay curve of La, Cr-codoped $SrTiO_3$ slightly increases compared to the one in N_2 environment, in contrast to the decay curve of La-doped $SrTiO_3$ which experiences a significant decrease (see Figure 5b), indicating the disappearance of electrons reactivity by La, Cr codoping. On the other hand, the signal intensity for the undoped $SrTiO_3$ increases noticeably, which might be attributed to the electron scavenging by O_2 (see Figure 5a), suggesting the exiguous holes feature in La, Cr-codoped $SrTiO_3$. In the presence of N_2 gas, the decay curves of both La-doped $SrTiO_3$ and La, Cr-codoped $SrTiO_3$ represents the population of electrons and holes. Based on the fitting results at 765 nm in 0-400 μs timescale, the decay constant of La, Cr-codoped $SrTiO_3$ is calculated to be 0.118 (see Figure 7c), which is much higher than that of La-doped $SrTiO_3$ ($k_{2,f} = 0.012$), indicating that La, Cr-codoped $SrTiO_3$ exhibited relatively shorter lifetime of photogenerated electrons.

The above results clarify that the recombination at Cr impurity level was not the main reason for the decrease in photocatalytic activity; since the Cr impurity level would absorb UV light and therefore inhibited the excitation of $SrTiO_3$, the activity under UV light was largely suppressed.

3.7 **Charge carriers dynamics**

According to the study using TAS, the charge carriers dynamics of the La-doped $SrTiO_3$ and La, Cr-codoped $SrTiO_3$ are proposed (Scheme 1a and 1b). After La doping, the TAS displays the distinctive feature of holes and electrons which cannot be observed on the undoped $SrTiO_3$. This distinction indicates that upon the illumination of probe light, the electrons were further excited to La 5d band which hybridized with the conduction band of $SrTiO_3$.[49, 51-52] As discussed above, the charge carriers lifetime of La-doped $SrTiO_3$ was relatively longer than the undoped $SrTiO_3$, implying that the La 5d orbital could contribute to prolonging lifetime of the charge carries, thus extending the interval for relaxation (see Figure 6 and Scheme 1a). After the codoping of La and Cr, the transient absorption spectra mainly exhibit the feature of electrons due to impurity level formed by Cr within the bandgap of $SrTiO_3$,[13] but not excited from the valence band of $SrTiO_3$. We experimentally observed that Cr d-orbital would act as such a recombination center through the oxidation of Cr^{3+} to Cr^{6+} by trapping 3 holes from the valence band of $SrTiO_3$. The reformation feature of Cr^{6+} to Cr^{3+} could not be observed in the micro second regime. However, stable photocatalytic activity of the material could be observed as shown in Figure 3a, suggesting the reformation of Cr^{6+} to Cr^{3+} in longer time regime (>800 μs) and thus the completion of the recombination process (see Scheme 1b).

Scheme 1. The proposed carrier dynamics from the transient absorption spectra in (a) La-doped $SrTiO_3$, (b) La, Cr-codoped $SrTiO_3$.

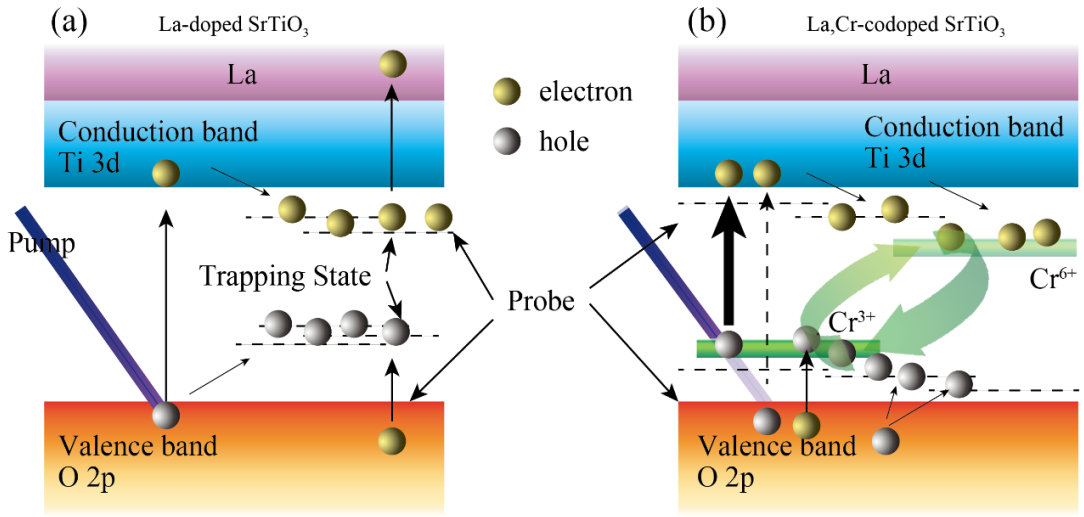

4. CONCLUSION

Based on the results of TAS, it can be inferred that La doping would extend the lifetime of photogenerated charge carriers due to the hybridization of La 5d band with conduction band of $SrTiO_3$ which could contribute to secure the excited electrons and thus increased total photocatalytic HER performance. After codoping of La and Cr, it was experimentally observed that on inert condition, Cr d-orbital would act as a recombination center through the oxidation state alteration. However, in the photocatalytic reaction environment where MeOH is existing as hole scavenger, the holes had the great tendency to be consumed by MeOH. Hence, the aforementioned recombination process could be avoided and should not be the main reason for the drastic decline in the photocatalytic activity. Interestingly, the majority of the electron excitation occurred from Cr impurity levels under UV light irradiation, which displayed less reactivity and lifetime, could account for decreasing the photocatalytic activity. Accordingly, in order to design a superior photocatalyst for effective solar energy harvesting, one should strive for enhancing the electron reactivity as well as retaining the excitation state of $SrTiO_3$.

ASSOCIATED CONTENT

Supporting Information. The following files are available free of charge.

Additional experimental data and results including atomic ratio and XPS spectra, transient decay curves at 825 nm and transient absorption spectra on 10% La, Cr-codoped $SrTiO_3$ (PDF)

AUTHOR INFORMATION

Corresponding Author

* Email: Jinhua.YE@nims.go.jp

ORCID

Jinhua Ye: 0000-0002-8105-8903

Present Addresses

‖ Present address: Evonik Industries AG, Rellinghauser Straße 1-11, Essen, 45128, Germany.

○ Present address: Hopa Kabelkonfektion GmbH & Co. KG, Am Pferdemarkt 61, Langenhagen, 30853, Germany

Notes

The authors declare no competing financial interest.

ACKNOWLEDGMENT

The work received the financial support from the World Premier International Research Center Initiative (WPI Initiative) on Materials Nanoarchitectonics (MANA) and KAKENHI(18H02065, 18K05207), MEXT, Japan. The authors also thank Dr. Jenny Schneider for her fruitful discussion.

REFERENCES

1. Zou, Z.; Ye, J.; Sayama, K.; Arakawa, H. Direct Splitting of Water under Visible Light Irradiation with an Oxide Semiconductor Photocatalyst. *Nature* **2001**, *414*, 625-627.

2. Kato, H.; Kudo, A. Visible-Light-Response and Photocatalytic Activities of TiO_2 and $SrTiO_3$ Photocatalysts Codoped with Antimony and Chromium. *J. Phys. Chem. B* **2002**, *106*, 5029-5034.

3. Liu, J. W.; Chen, G.; Li, Z. H.; Zhang, Z. G. Electronic Structure and Visible Light Photocatalysis Water Splitting Property of Chromium-Doped $SrTiO_3$. *J. Solid State Chem.***2006**, *179*, 3704-3708.

4. Ouyang, S.; Tong, H.; Umezawa, N.; Cao, J.; Li, P.; Bi, Y.; Zhang, Y.; Ye, J. Surface-Alkalinization-Induced Enhancement of Photocatalytic H_2 Evolution over $SrTiO_3$-Based Photocatalysts. *J. Am. Chem. Soc.* **2012**, *134*, 1974-7.

5. Tong, H.; Ouyang, S.; Bi, Y.; Umezawa, N.; Oshikiri, M.; Ye, J. Nano-Photocatalytic Materials: Possibilities and Challenges. *Adv. Mater.* **2012**, *24*, 229-251.

6. Meng, X.; Zuo, G.; Zong, P.; Pang, H.; Ren, J.; Zeng, X.; Liu, S.; Shen, Y.; Zhou, W.; Ye, J. A Rapidly Room-Temperature-Synthesized Cd/ZnS:Cu Nanocrystal Photocatalyst for Highly Efficient Solar-Light-Powered CO_2 Reduction. Appl. Catal. B: Environ. **2018**, *237*, 68-73.

7. Li, P.; Ouyang, S.; Xi, G.; Kako, T.; Ye, J. The Effects of Crystal Structure and Electronic Structure on Photocatalytic H_2 Evolution and CO_2 Reduction over Two Phases of Perovskite-Structured $NaNbO_3$. *J. Phys. Chem. C* **2012**, *116*, 7621-7628.

8. Kang, Q.; Wang, T.; Li, P.; Liu, L.; Chang, K.; Li, M.; Ye, J. Photocatalytic Reduction of Carbon Dioxide by Hydrous Hydrazine over Au–Cu Alloy Nanoparticles Supported on $SrTiO_3/TiO_2$ Coaxial Nanotube Arrays. *Angew. Chem.* **2015**, *127*, 855-859.

9. Yan, S. C.; Ouyang, S. X.; Gao, J.; Yang, M.; Feng, J. Y.; Fan, X. X.; Wan, L. J.; Li, Z. S.; Ye, J. H.; Zhou, Y.; Zou, Z. G. A Room-Temperature Reactive-Template Route to Mesoporous $ZnGa_2O_4$ with Improved Photocatalytic Activity in Reduction of CO_2. *Angew. Chem. Int. Ed.* **2010**, *49*, 6400-6404.

10. Xie, K.; Umezawa, N.; Zhang, N.; Reunchan, P.; Zhang, Y.; Ye, J. Self-Doped $SrTiO_{3-\delta}$ Photocatalyst with Enhanced Activity for Artificial Photosynthesis under Visible Light. *Energy Environ. Sci.* **2011**, *4*, 4211-4219.

11. Li, H.; Shang, J.; Ai, Z.; Zhang, L. Efficient Visible Light Nitrogen Fixation with BiOBr Nanosheets of Oxygen Vacancies on the Exposed {001} Facets. *J. Am. Chem. Soc.* **2015**, *137*, 6393-6399.

12. Wang, S.; Hai, X.; Ding, X.; Chang, K.; Xiang, Y.; Meng, X.; Yang, Z.; Chen, H.; Ye, J. Light-Switchable Oxygen Vacancies in Ultrafine Bi_5O_7Br Nanotubes for Boosting Solar-Driven Nitrogen Fixation in Pure Water. *Adv. Mater.* **2017**, *29*, 1701774.

13. Tonda, S.; Kumar, S.; Anjaneyulu, O.; Shanker, V. Synthesis of Cr and La-Codoped $SrTiO_3$ Nanoparticles for Enhanced Photocatalytic Performance under Sunlight Irradiation. *Phys. Chem. Chem. Phys.* **2014**, *16*, 23819-28.

14. Hirano, K.; Suzuki, E.; Ishikawa, A.; Moroi, T.; Shiroishi, H.; Kaneko, M. Sensitization of TiO_2 Particles by Dyes to Achieve H_2 Evolution by Visible Light. *J. Photochem. Photobiol. A: Chem.* **2000**, *136*, 157-161.

15. Youngblood, W. J.; Lee, S.-H. A.; Maeda, K.; Mallouk, T. E. Visible Light Water Splitting Using Dye-Sensitized Oxide Semiconductors. *Acc. Chem. Res.* **2009**, *42*, 1966-1973.

16. Kato, H.; Asakura, K.; Kudo, A. Highly Efficient Water Splitting into H_2 and O_2 over Lanthanum-Doped $NaTaO_3$ Photocatalysts with High Crystallinity and Surface Nanostructure. *J. Am. Chem. Soc.* **2003**, *125*, 3082-3089.

17. Liu, L.; Li, P.; Adisak, B.; Ouyang, S.; Umezawa, N.; Ye, J.; Kodiyath, R.; Tanabe, T.; Ramesh, G. V.; Ueda, S.; Abe, H. Gold Photosensitized $SrTiO_3$ for Visible-Light Water Oxidation Induced by Au Interband Transitions. *J. Mater. Chem. A* **2014**, *2*, 9875.

18. Wang, D.; Ye, J.; Kako, T.; Kimura, T. Photophysical and Photocatalytic Properties of $SrTiO_3$ Doped with Cr Cations on Different Sites. *J. Phys. Chem. B* **2006**, *110*, 15824-15830.

19. Serpone, N.; Lawless, D.; Disdier, J.; Herrmann, J.-M. Spectroscopic, Photoconductivity, and Photocatalytic Studies of TiO_2 Colloids: Naked and with the Lattice Doped with Cr^{3+}, Fe^{3+}, and V^{5+} Cations. *Langmuir* **1994**, *10*, 643-652.

20. Xie, T.; Sun, X.; Lin, J. Enhanced Photocatalytic Degradation of RhB Driven by Visible Light-Induced MMCT of Ti(IV)−O−Fe(II) Formed in Fe-Doped $SrTiO_3$. *J. Phys. Chem. C* **2008**, *112*, 9753-9759.

21. Wu, G.; Li, P.; Xu, D.; Luo, B.; Hong, Y.; Shi, W.; Liu, C. Hydrothermal Synthesis and Visible-Light-Driven Photocatalytic Degradation for Tetracycline of Mn-Doped $SrTiO_3$ Nanocubes. *Appl. Surf. Sci.* **2015**, *333*, 39-47.

22. Asahi, R.; Morikawa, T.; Ohwaki, T.; Aoki, K.; Taga, Y. Visible-Light Photocatalysis in Nitrogen-Doped Titanium Oxides. *Science* **2001**, *293*, 269-271.

23. Maeda, K.; Domen, K. New Non-Oxide Photocatalysts Designed for Overall Water Splitting under Visible Light. *J. Phys. Chem. C* **2007**, *111*, 7851-7861.

24. Teruhisa, O.; Takahiro, M.; Michio, M. Photocatalytic Activity of S-Doped TiO_2 Photocatalyst under Visible Light. *Chem. Lett.* **2003**, *32*, 364-365.

25. Yamakata, A.; Kawaguchi, M.; Murachi, R.; Okawa, M.; Kamiya, I. Dynamics of Photogenerated Charge Carriers on Ni- and Ta-Doped $SrTiO_3$ Photocatalysts Studied by Time-Resolved Absorption and Emission Spectroscopy. *J. Phys. Chem. C* **2016**, *120*, 7997-8004.

26. Fan, X.; Chen, X.; Zhu, S.; Li, Z.; Yu, T.; Ye, J.; Zou, Z. The Structural, Physical and Photocatalytic Properties of the Mesoporous Cr-Doped TiO_2. *J. Mol. Catal. A: Chem.* **2008**, *284*, 155-160.

27. Niishiro, R.; Kato, H.; Kudo, A. Nickel and Either Tantalum or Niobium-Codoped TiO_2 and $SrTiO_3$ Photocatalysts with Visible-Light Response for H_2 or O_2 Evolution from Aqueous Solutions. *Phys. Chem. Chem. Phys.* **2005**, *7*, 2241-2245.

28. Takata, T.; Domen, K. Defect Engineering of Photocatalysts by Doping of Aliovalent Metal Cations for Efficient Water Splitting. *J. Phys. Chem. C* **2009**, *113*, 19386-19388.

29. Hoffmann, M. R.; Martin, S. T.; Choi, W.; Bahnemann, D. W. Environmental Applications of Semiconductor Photocatalysis. *Chem. Rev.* **1995**, *95*, 69-96.

30. Schneider, J.; Matsuoka, M.; Takeuchi, M.; Zhang, J.; Horiuchi, Y.; Anpo, M.; Bahnemann, D. W. Understanding TiO_2 Photocatalysis: Mechanisms and Materials. *Chem. Rev.* **2014**, *114*, 9919-9986.

31. Schneider, J.; Nikitin, K.; Wark, M.; Bahnemann, D. W.; Marschall, R. Improved Charge Carrier Separation in Barium Tantalate Composites Investigated by Laser Flash Photolysis. *Phys. Chem. Chem. Phys.* **2016**, *18*, 10719-26.

32. Yamakata, A.; Vequizo, J. J. M.; Matsunaga, H. Distinctive Behavior of Photogenerated Electrons and Holes in Anatase and Rutile TiO_2 Powders. *J. Phys. Chem. C* **2015**, *119*, 24538-24545.

33. Sieland, F.; Schneider, J.; Bahnemann, D. W. Fractal Charge Carrier Kinetics in TiO_2. *J. Phys. Chem. C* **2017**, *121*, 24282-24291.

34. Yamakata, A.; Ishibashi, T.; Kato, H.; Kudo, A.; Onishi, H. Photodynamics of $NaTaO_3$ Catalysts for Efficient Water Splitting. *J. Phys. Chem. B* **2003**, *107*, 14383-14387.

35. Nishioka, S.; Hyodo, J.; Vequizo, J. J. M.; Yamashita, S.; Kumagai, H.; Kimoto, K.; Yamakata, A.; Yamazaki, Y.; Maeda, K. Homogeneous Electron Doping into Nonstoichiometric Strontium Titanate Improves Its Photocatalytic Activity for Hydrogen and Oxygen Evolution. *ACS Catal.* **2018**, *8*, 7190-7200.

36. Yamakata, A.; Vequizo, J. J. M.; Kawaguchi, M. Behavior and Energy State of Photogenerated Charge Carriers in Single-Crystalline and Polycrystalline Powder $SrTiO_3$ Studied by Time-Resolved Absorption Spectroscopy in the Visible to Mid-Infrared Region. J. *Phys. Chem. C* **2015**, *119*, 1880-1885.

37. Yamakata, A.; Kawaguchi, M.; Nishimura, N.; Minegishi, T.; Kubota, J.; Domen, K. Behavior and Energy States of Photogenerated Charge Carriers on Pt- or CoO_x-Loaded $LaTiO_2N$ Photocatalysts: Time-Resolved Visible to Mid-Infrared Absorption Study. *J. Phys. Chem. C* **2014**, *118*, 23897-23906.

38. Furuhashi, K.; Jia, Q.; Kudo, A.; Onishi, H. Time-Resolved Infrared Absorption Study of $SrTiO_3$ Photocatalysts Codoped with Rhodium and Antimony. *J. Phys. Chem. C* **2013**, *117*, 19101-19106.

39. Umebayashi, T.; Yamaki, T.; Itoh, H.; Asai, K. Analysis of Electronic Structures of 3d Transition Metal-Doped TiO_2 Based on Band Calculations. *J. Phys. Chem. Solids* **2002**, *63*, 1909-1920.

40. Jia, Y.; Shen, S.; Wang, D.; Wang, X.; Shi, J.; Zhang, F.; Han, H.; Li, C. Composite $Sr_2TiO_4/SrTiO_3$(La, Cr) Heterojunction Based Photocatalyst for Hydrogen Production under Visible Light Irradiation. *J. Mater. Chem. A* **2013**, *1*, 7905-7912.

41. Ishii, T.; Kato, H.; Kudo, A. H_2 Evolution from an Aqueous Methanol Solution on $SrTiO_3$ Photocatalysts Codoped with Chromium and Tantalum Ions under Visible Light Irradiation. *J. Photochem. Photobiol. A: Chem.* **2004**, *163*, 181-186.

42. Reunchan, P.; Ouyang, S.; Umezawa, N.; Xu, H.; Zhang, Y.; Ye, J. Theoretical Design of Highly Active $SrTiO_3$-Based Photocatalysts by a Codoping Scheme towards Solar Energy Utilization for Hydrogen Production. *J. Mater. Chem. A* **2013**, *1*, 4221-4227.

43. Goldschmidt, V. M. Die Gesetze der Krystallochemie. *Naturwissenschaften* **1926**, *14*, 477-485.

44. Peña, M. A.; Fierro, J. L. G. Chemical Structures and Performance of Perovskite Oxides. *Chem. Rev.* **2001**, *101*, 1981-2018.

45. Borgarello, E.; Kiwi, J.; Graetzel, M.; Pelizzetti, E.; Visca, M. Visible Light Induced Water Cleavage in Colloidal Solutions of Chromium-Doped Titanium Dioxide Particles. *J. Am. Chem. Soc.* **1982**, *104*, 2996-3002.

46. Mackor, A.; Blasse, G. Visible-Light Induced Photocurrents in $SrTiO_3$-$LaCrO_3$ Single-Crystalline Electrodes. *Chem. Phys. Lett.* **1981**, *77*, 6-8.

47. Yamakata, A.; Ishibashi, T.; Onishi, H. Water- and Oxygen-Induced Decay Kinetics of Photogenerated Electrons in TiO_2 and Pt/TiO_2: A Time-Resolved Infrared Absorption Study. *J. Phys. Chem. B* **2001**, *105*, 7258-7262.

48. Yamakata, A.; Ishibashi, T.; Onishi, H. Electron- and Hole-Capture Reactions on Pt/TiO_2 Photocatalyst Exposed to Methanol Vapor Studied with Time-Resolved Infrared Absorption Spectroscopy. *J. Phys. Chem. B* **2002**, *106*, 9122-9125.

49. Shanthi, N.; Sarma, D. D. Electronic structure of electron doped $SrTiO_3$: $SrTiO_{3-\delta}$ and $Sr_{1-x}La_xTiO_3$. *Phys. Rev. B* **1998**, *57*, 2153-2158.

50. Xiuli, W.; Andreas, K.; Xiaoe, L.; Savio, J. A. M. ; Philip, J. T. R.; Junwang, T.; Ivan, P. P.; James, R. D. Transient Absorption Spectroscopy of Anatase and Rutile: Impact of Morphology and Phase on Photocatalytic Activity. *J. Phys. Chem. C* **2015**, *119*, 10439-10447.

51. El-Mellouhi, F.; Brothers, E. N.; Lucero, M. J.; Bulik, I. W.; Scuseria, G. E. Structural phase transitions of the metal oxide perovskites $SrTiO_3$, $LaAlO_3$, and $LaTiO_3$studied with a screened hybrid functional. *Phys. Rev. B* **2013**, *87*, 035107.

52. Biswas, A.; Li, N.; Jung, M. H.; Lee, Y. W.; Kim, J. S.; Jeong, Y. H. La doped $SrTiO_3$ thin films on $SrLaAlO_4$ (001) as transparent conductor. *J. Appl. Phys.* **2013**, *113*, 183711.

53. Maruyama, M.; Iwase, A.; Kato, H.; Kudo, A.; Onishi, H., Time-Resolved Infrared Absorption Study of NaTaO3 Photocatalysts Doped with Alkali Earth Metals. *J. Phys. Chem. C* **2009**, 113 (31), 13918-13923.

Table of Contents Graphics